Separatrix-map analysis of chaotic transport in planar periodic vortical flows

Taehoon Ahn and Seunghwan Kim
Departments of Mathematics and Physics, Basic Science Research Institute, POSTECH, Pohang 790-784, Korea
(Received 16 August 1993)

We have studied chaotic transport in a two-dimensional periodic vortical flow under a time-dependent perturbation with period T, where the global diffusion occurs along the stochastic web. By using the Melnikov method we construct the separatrix map describing the approximate dynamics near the saddle separatrices. Focusing on small T, the width of the stochastic layer is calculated analytically using the residue criterion and the diffusion constant is computed using the random phase assumption and the theory of correlated random walks. The analytical results are in good agreement with the results of two different types of numerical simulations: integrations of Hamilton's equation of motion and iterations of the separatrix map, which establishes the validity of the use of the separatrix map.

PACS number(s): 47.52.+j, 47.20.−k, 05.60.+w, 05.45.+b

I. INTRODUCTION

Recently the global transport and mixing in the problems of planar fluids have been studied intensively using the framework of dynamical system theory, where interesting physical quantities like mass or heat can be described to some degree of approximation as moving with the fluid particle [1–3].

When the flow is laminar, the velocity vector field $v(x,y,t)$ of a two-dimensional incompressible inviscid fluid flow can be determined from a stream function $\Psi(x,y,t)$ and the equations for an infinitesimal fluid element (called a *fluid particle*) become a Hamiltonian dynamical system where the stream function plays the role of the Hamiltonian. It is now well established that for the time-dependent stream function the particle trajectories can display chaotic dynamics, even though the Eulerian flow is laminar [4]. Such a flow is said to exhibit *chaotic advection.*

In this paper we consider the planar periodic vortical flow in which there are four hyperbolic saddle points connected by heteroclinic orbits [5]. This is an interesting model for certain convection problems as well as the axisymmetric Taylor vortex flow and the Rossby waves of geophysical fluid dynamics [6]. With a time-periodic perturbation the separatrices break down and form a globally connected stochastic layer (called the *stochastic web*). Fluid particles diffuse chaotically along the stochastic layer, which can be regarded as a stochastic process in a coarse-grained scale. This stochastic transport occurs on the global scale along the two-dimensional squarelike lattice of the stochastic web and is studied in terms of the *separatrix map.*

The separatrix map is an approximate map describing the dynamics of the energy and the phase near the separatrices of the periodic Hamiltonian system, first introduced by Chirikov [7], which allows an efficient and systematic study of dynamics near the stochastic web. Escande first used the separatrix map for the transport problem [8] and Weiss and Knobloch used it to study numerically the anomalous diffusion of the fluid particle along modulated traveling waves [1]. In spite of the wide usage of the separatrix map for studying Hamiltonian transport problems [8–10], however, the validity of the separatrix-map analysis has not been firmly established yet. In this paper, we test the validity for the separatrix map as a general method for studying transport in a Hamiltonian system with the planar periodic vortical flow as an example. We follow Weiss and Knobloch to construct the separatrix map for the planar periodic vortical flow and use it to estimate the width of the stochastic web and the diffusion constant analytically, extending the analysis of Lichtenberg and Wood on the Hamiltonian system of charged particles in a magnetic field [9]. Analytical results are in good agreement with numerical results from direct integration of the original Hamiltonian vector field and iterations of the separatrix map.

First we compute the analytical form of the separatrix map for the energy and phase coordinates, by introducing a set of Poincaré sections and applying the Melnikov theory. We show that the separatrix map provides a first order approximation to true dynamics near the separatrices. We also show that if the period of the perturbation T is small, the stochastic layer is sufficiently wider than the splittings of stable and unstable manifolds and the separatrix map can describe the structure of the stochastic layer away from the separatrices very well. We find that Greene's residue criterion [11] for the separatrix map gives a quite accurate estimate for the width of the stochastic layer.

A problem may arise when the orbit approaches the separatrix since the error of the separatrix map grows indefinitely [12]. We will show that this can be overcome by assuming that the phase is a random variable for dynamics near the separatrix. This model with a random phase is different from the model of Lichtenberg and Wood where both the energy and the phase are random variables. We find numerically that the random phase model gives the same statistics for separatrix crossings as ones from simple iterations of the separatrix map and direct integrations of the original Hamiltonian equation, so that the averaged quantities such as the diffusion con-

stant can be explored through the random phase model. The random phase assumption leads to the two-dimensional correlated random walks [13], where in a coarse grained level the global dynamics can be described by stochastic jumps from one cell to another. The theory of correlated random walks with a correction due to elliptic islands in the stochastic layer gives an analytic estimate of the diffusion constant to the first order.

For area-preserving maps, two methods have been widely used for studying transport. One is the Markov chain model suggested by Mackay and co-workers [14,15] and the other is the lobe dynamics developed by Rom-Kedar, Leonard, and Wiggins [16,17]. In the Markov chain model, the phase space is divided into several regions separated by partial barriers and transport between the regions is modeled as a Markov chain, in which each region is represented by the states, and the transition probabilities are proportional to the area of the turnstile lobes. Using the lobe dynamics, one can compute the flux across the separatrix and transport rates by calculating the area of intersections between images of two turnstile lobes. These two methods, when applied to the time-T Poincaré map, require time-consuming numerical evaluation of the area of the turnstile lobes for each parameter values [18], so that it is difficult to apply them to study the asymptotic transport dynamics such as the global diffusion because of long computation time and large numerical errors. The separatrix map has the advantage that its numerical iteration is quite rapid because the map depends only on the Melnikov function and the period of the unperturbed orbits that can be calculated and stored in advance even in the absence of analytic expressions for them [1]. In particular, with the random phase assumption the statistical properties of transport can be easily obtained by simple iterations of the separatrix map. Moreover, as the period of perturbation T decreases, the advantages of using the separatrix map increases since one iteration of the separatrix map corresponds to a large number of iterations of the time-T Poincaré map.

In Sec. II, we introduce the model Hamiltonian describing the flow with the vortex lattice with saddle connections under time-periodic perturbations. We show the formation of the globally connected stochastic web by computing the Melnikov function and applying the Smale-Birkhoff theorem. We also construct the separatrix map and provide an error analysis on the separtrix map. In Sec. III, we describe the structure of the global stochastic layer and calculate the analytical form for the width of the stochastic layer by using the residue criterion on the separatrix map. In Sec. IV, based on the random phase assumption, the diffusion constant is computed by applying the theory of correlated random walks. We compare analytical results with those from numerical simulations. Finally, we end with concluding remarks.

II. THE MELNIKOV METHOD AND THE SEPARATRIX MAP

A. The model

As a model for a two-dimensional time-dependent flow we consider the following stream function [5]:

$$\Psi(x,y,t)=H(x,y)+\varepsilon H_1(x,y,t) , \tag{1}$$

where

$$H(x,y)=\frac{1}{2\pi}\sin(2\pi x)\cos(2\pi y) ,$$
$$H_1(x,y,t)=\frac{1}{2\pi}\cos(\omega t)[\sin(2\pi y)+\cos(2\pi x)] . \tag{2}$$

This stream function corresponds to the near-integrable Hamiltonian system with time-dependent perturbation of period $T=2\pi/\omega$ and the equations of motion for fluid particles are given by

$$\begin{bmatrix}\dot{x}\\ \dot{y}\end{bmatrix}=\begin{bmatrix}-\sin(2\pi x)\sin(2\pi y)+\varepsilon\cos(2\pi y)\cos(\omega t)\\ -\cos(2\pi x)\cos(2\pi y)+\varepsilon\sin(2\pi x)\cos(\omega t)\end{bmatrix} , \tag{3}$$

or, in a vector form,

$$\dot{q}=JF(q)+\varepsilon G(x,y,t) , \tag{4}$$

where

$$q=\begin{bmatrix}x\\ y\end{bmatrix},\quad J\equiv\begin{bmatrix}0 & 1\\ -1 & 0\end{bmatrix},\quad F\equiv\begin{bmatrix}\frac{\partial H}{\partial x}\\ \frac{\partial H}{\partial y}\end{bmatrix} ,$$

$$\text{and } G\equiv\begin{bmatrix}\frac{\partial H_1}{\partial y}\\ -\frac{\partial H_1}{\partial x}\end{bmatrix} .$$

This equation describes a two-dimensional periodic vortical flow under time-dependent perturbation. This flow is obviously doubly periodic, yielding a flow on the torus. Viewed as a flow on the torus, the unperturbed system is an integrable Hamiltonian system with heteroclinic orbits connecting four saddle points. On the torus, there exist four vorticies whose boundaries are the heteroclinic orbits. The values of H are zero on the heteroclinic orbits and have a definite sign for each vortex. The phase portrait of the unperturbed system is shown in Fig. 1. Under the periodic perturbation the heteroclinic connections break down and the stable and unstable manifolds between two adjacent saddle points in general do not coincide with each other and intersect transversally.

B. The Melnikov method

For a system with a saddle connection under a time-dependent perturbation Melnikov devised a method for finding the transverse intersection of stable and unstable manifolds [19]. Let $q_s(t)$ be the heteroclinic orbit of the unperturbed system. The distance between the stable and unstable manifolds along the direction normal to the unperturbed heteroclinic orbit at $q_s(-t_0)$ is given by

$$d(t_0,\varepsilon)=\varepsilon\frac{M(t_0)}{\|F(q_s(-t_0))\|} , \tag{5}$$

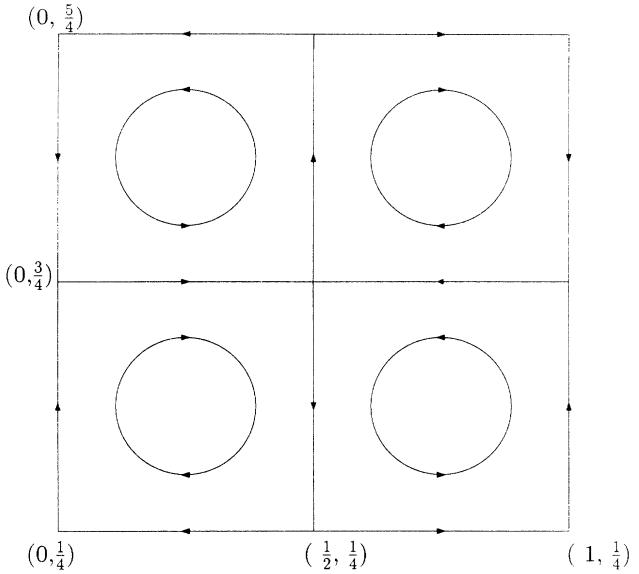

FIG. 1. The phase space of the unperturbed system in Eq. (3) with $\varepsilon=0$. The system is doubly periodic in x and y and the separatrices are globally connected.

where $\| \ \|$ is the Euclidean norm in $\mathbb{R}^2$ and $M(t_0)$ is the Melnikov function

$$M(t_0)=\int_{-\infty}^{\infty} F\cdot G(q_s(t),t+t_0)dt \ . \tag{6}$$

The Melnikov theory says that if the Melnikov function has a simple zero, then the stable and unstable manifolds intersect transversely at $q_s(-t_0)+O(\varepsilon)$ [20].

The Melnikov function for our Hamiltonian vector field can be computed explicitly. Along all unperturbed horizontal connections we have

$$\sin(2\pi x)=\pm\frac{2\exp(-2\pi t)}{1+\exp(-4\pi t)} \tag{7}$$

and along all vertical connections

$$\cos(2\pi y)=\pm\frac{2\exp(-2\pi t)}{1+\exp(-4\pi t)} \ . \tag{8}$$

Then the Melnikov function in Eq. (6) becomes

$$\begin{aligned} M^{\pm}(t_0)&=\pm\int_{-\infty}^{\infty}\frac{\exp(-4\pi t)}{[1+\exp(-4\pi t)]^2}\cos\omega(t+t_0)dt \\ &=\pm\frac{\omega}{4\pi}\frac{1}{\sinh\left[\frac{\omega}{4}\right]}\cos(\omega t) \ , \end{aligned} \tag{9}$$

or

$$M^{\pm}(t_0)=\pm M_0(T)\cos\left[\frac{2\pi}{T}t_0\right], \quad T=\frac{2\pi}{\omega} \tag{10}$$

where

$$M_0(T)=\frac{1}{2T}\operatorname{csch}\left[\frac{\pi}{2T}\right] \ . \tag{11}$$

Hence we see that the Melnikov function is periodic with period T and has two simple zeros per period and, therefore, by the Melnikov theory the stable and the unstable manifolds intersect transversely. If the system has a transversal intersection of the stable and the unstable manifolds, the Smale-Birkhoff homoclinic theorem proves the existence of chaotic orbits [21,22]. It is straightforward to extend this theorem to the heteroclinic case [5], to prove that our system has a chaotic orbit under a periodic perturbation $H_1(q,t)$. In fact, the chaotic orbits form a stochastic layer along the separatrices and the fluid particle can be globally diffused along the connected stochastic layer. We note that the T dependence of $M_0(T)$ is of the form, $\exp(-1/T)$, as proved by Holmes Marsden, and Scheurle [23]. Therefore, the separatrix splittings are exponentially small in the small T limit, yielding the exponentially thin stochastic web.

C. The separatrix map

As discussed in the Introduction, long-time asymptotic behavior of chaotic transport can be efficiently studied by the separatrix-map method. In order to construct the separatrix map, we choose two saddle points, $q_0=(0,\frac{1}{4})$ and $q_1=(0,\frac{3}{4})$, connected by the heteroclinic orbit

$$q_s(t)=\left[0,\frac{1}{2\pi}\arccos\left[-\frac{2\exp(-2\pi t)}{1+\exp(-4\pi t)}\right]\right] \ . \tag{12}$$

We also choose three different surfaces of section

$$\begin{aligned} \Sigma^t&=\{(x,y)\,|\,|x|<\delta,y=\tfrac{1}{2}\} \ , \\ \Sigma_0^H&=\{(x,y)\,\|x|<\delta,y=\tfrac{1}{4}+|x|\} \ , \\ \Sigma_1^H&=\{(x,y)\,\|x|<\delta,y=\tfrac{3}{4}-|x|\} \ , \end{aligned} \tag{13}$$

where δ is a small positive value. Suppose that these sections are chosen for each separatrix. Suppose also that $q(t)$ is a perturbed orbit such that $q(s_n)\in\Sigma_0^H$, $q(t_n)\in\Sigma^t$, $q(s_{n+1})\in\Sigma_1^H$, and $q(t)$ crosses Σ^t of the next separatrix at time t_{n+1}, as shown in Fig. 2. The change of the energy H from $q(s_n)$ to $q(s_{n+1})$ along $q(t)$ is given by

$$\Delta H=\int_{s_n}^{s_{n+1}}\frac{dH}{dt}dt=\varepsilon\int_{s_n}^{s_{n+1}}F\cdot G(q(t),t)dt \ . \tag{14}$$

From the relation $dx/dt=\partial H/\partial y$, t_{n+1} is given by

$$t_{n+1}=t_n+\int_{q(t_n)}^{q(t_{n+1})}\frac{\partial H}{\partial y}(q(t),t)^{-1}dx \ . \tag{15}$$

We call the map $S_e:(H,t_n)\to(H+\Delta H,t_{n+1})$ the *exact separatrix map,* which describes the exact dynamics of the energy H and the time (or phase) t. Here (H,t) plays the role of a new coordinate system in the planar fluid space near the separatrix. Now we approximate $q(t)$ by the heteroclinic orbit $q_s(t)$ and $t_{n+1}-t_n$ by the period of an unperturbed solution $q_0(t)$ with $H_0=H+\Delta H$. Then $\Delta H\simeq\varepsilon M^{\pm}(t_n)$, where $M^{\pm}(t_n)$ is the Melnikov function in Eq. (10). Then an (approximate) separatrix map is given by

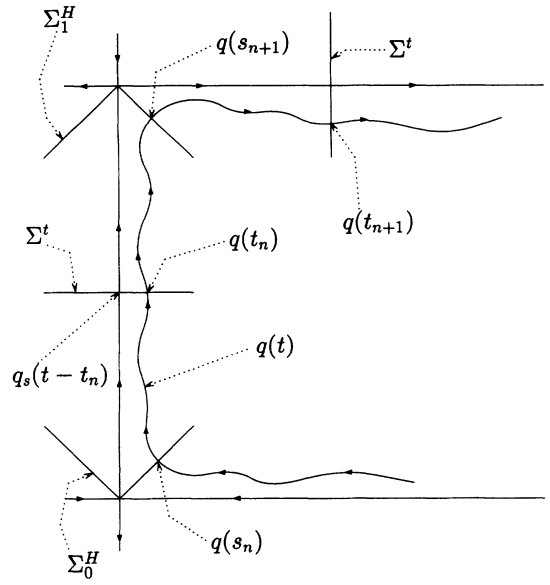

FIG. 2. A sketch for the construction of the separatrix map. The orbit $q_s(t)$ is the heteroclinic orbit of the unperturbed system and $q(t)$ a perturbed orbit. The sections Σ^H and Σ^t are the Poincaré sections for the coordinates (H,t).

$$\begin{bmatrix} H_{n+1} \\ t_{n+1} \end{bmatrix} = S^{\pm}(H_n,t_n) = \begin{bmatrix} H_n + \varepsilon M^{\pm}(t_n) \\ t_n + \frac{1}{4}T(H_n + \varepsilon M^{\pm}(t_n)) \end{bmatrix}, \tag{16}$$

where $T(h)$ is a period of an unperturbed orbit with $H=h$. It can be shown that

$$S_e(H_n,t_n) = S^{\pm}(H_n,t_n) + \begin{bmatrix} O(\varepsilon^2) \\ O(\varepsilon) \end{bmatrix} \tag{17}$$

for $|H_n| = O(\varepsilon)$. Therefore, $S^{\pm}$ is valid for small ε, that is, near the separatrix [12]. We note that if T is small, then the change of H is exponentially small, so that the validity of $S^{\pm}$ does not appear to be justified. However, the numerical observation shows that $\mathcal{O}(\varepsilon^2)$ error term is also exponentially small, justifying the use of $S^{\pm}$. However, this issue is a mathematically difficult problem and is not fully understood yet [23–25].

Near the separatrices a straightforward computation for our system in Eq. (3) yields

$$T(H) = \frac{2}{\pi}K(1-4\pi^2H^2) \simeq \frac{2}{\pi}\ln\frac{2}{\pi|H|} \quad \text{for } |H| \ll 1 , \tag{18}$$

where $K(\ )$ is the complete elliptic integral of the first kind. Therefore, we get the separatrix map for our system

$$\begin{bmatrix} H' \\ t' \end{bmatrix} = S^{\pm}(H,t) = \begin{bmatrix} H \pm \varepsilon M_0(T)\cos\left[\frac{2\pi}{T}\right] \\ t + \frac{1}{2\pi}\ln\frac{2}{\pi|H'|} \end{bmatrix}, \tag{19}$$

which is used throughout the rest of the paper to explore chaotic transport.

III. THE STRUCTURE AND THE WIDTH OF THE STOCHASTIC LAYER

A. Properties of the separatrix map

In order to study the dynamics in the stochastic layer, it is important to understand the structure of the stochastic layer first. The stochastic layer is composed of not only chaotic orbits but also other complex structures such as elliptic islands which exist away from the separatrices and become relevant to transport when T is small. We will show later that these structures can be described very well by the separatrix map. From Eq. (19) we see that the value of H changes roughly by the amount $\varepsilon M_0(T)$ as a fluid particle moves along a separatrix. When T is small, we will show later that the width of the stochastic layer is significantly larger than $\varepsilon M_0(T)$. Therefore the values of H have a definite sign for a long time even for chaotic orbits, which corresponds to oscillating dynamics confined in one cell. In order to study oscillations in a single cell, it is convenient to introduce the *composite separatrix map* $S = S^+ \circ S^- \circ S^- \circ S^+$ because one iteration of S corresponds to one oscillation confined in a cell *if* the sign of H does not change. The map $S^{\pm}$ are defined on the cylinder with a form similar to the area-preserving twist map [26]. The map $S^{\pm}$ are different from the twist map in the sense that it has a logarithmic singularity at $H'=0$ and its twist conditions depend on the sign of H'. However, similarly to the area-preserving twist map, $S^{\pm}$ have generating functions given by

$$G(t,t') = \mathrm{sgn}(H')\frac{1}{\pi^2}e^{2\pi(t-t')} \mp \frac{\varepsilon}{4\pi}\mathrm{csch}\left[\frac{\pi}{2T}\right]\sin\frac{2\pi}{T}t , \tag{20}$$

where $\mathrm{sgn}(H')$ denotes a sign of H' and $G(t,t')$ satisfies

$$H = \frac{\partial G}{\partial t}(t,t'), \quad H' = -\frac{\partial G}{\partial t'}(t,t') . \tag{21}$$

With the help of generating functions, it can be shown that the twist map has complex dynamical structures with periodic orbits, quasiperiodic orbits forming invariant circles, chaotic orbits, and cantori [26]. The cantori are the invariant Cantor sets in which the motion is quasiperiodic and they typically exist in the stochastic layer [27–29]. With the generating function in Eq. (20), the method of proving the existence of periodic and quasiperiodic orbits for the twist map [26] can be easily applied to the map S to show that there exist periodic orbits and quasiperiodic orbits which do not cross the separatrix, so that elliptic islands and invariant circles are confined in one cell.

B. Periodic orbits and residues

The composite separatrix map S has infinitely many fixed points of rotation number $2m/1$ near the separatrix $(\bar{H},\bar{t})$, satisfying

$$M^{\pm}(\bar{t})=0 \text{ and } T(\bar{H})=2mT \ , \tag{22}$$

where m is a large positive integer, or, equivalently,

$$\bar{t}=\frac{T}{4} \text{ or } \frac{3}{4}T \text{ and } \bar{H}=\frac{2}{\pi}\exp\left[-\frac{m\pi T}{2}\right] . \tag{23}$$

The map S also has fixed points of rotation number $(2m+1)/1$ near $(\bar{H},\bar{t})$, where

$$M^{+}(\bar{t})+M^{-}\left[\bar{t}+\frac{mT}{4}\right]+M^{-}\left[\bar{t}+\frac{mT}{2}\right]+M^{+}\left[\bar{t}+\frac{3mT}{4}\right]=0$$

and

$$T(\bar{H})=(2m+1)T \ . \tag{24}$$

These two classes of the fixed points of rotation number $m/1$ correspond to the zeros of $M^{m/1}(t)$, the subharmonic Melnikov function [30], since

$$M^{m/1}(t)\simeq M^{+}(t)+M^{-}\left[t+\frac{mT}{4}\right]+M^{-}\left[t+\frac{mT}{2}\right]+M^{+}\left[t+\frac{3mT}{4}\right] , \tag{25}$$

for sufficiently large m. By using the subharmonic Melnikov theory it can be proved from the implicit function theorem that a simple zero of $M^{m/1}(t)$ corresponds to a periodic orbit with period mT. Therefore the fixed points of S correspond to periodic orbits of the original Hamiltonian flow. In Fig. 3 we plot the phase portraits of S and the time-T Poincaré map near a saddle point, whose elliptic island structures show that correspondence between the resonance bands of the time-T Poincaré map and the fixed points of S.

In order to know the stability of a periodic orbit of S, it is necessary to check the residue of the periodic orbit. Given a periodic orbit of period q, its residue R is defined by

$$R=\tfrac{1}{4}(2-\mathrm{Tr}[B^{q}]) , \tag{26}$$

where B^{q} is the Jacobian matrix of the qth iterate of the map S. For the twist map it is known that for each rational p/q there exists at least one periodic orbit of rotation number p/q with non-negative residue $R_{p/q}$. For the map S, numerical observations indicate that the non-negative residues of the periodic points of sufficiently large rotation number are greater than 1, so that they are hyperbolic. If the rotation number is not sufficiently large or periodic points of S are sufficiently far away from the separatrix, their non-negative residues are less than 1, that is, they are elliptic, so that such fixed points of S correspond to resonance bands of the time-T Poincaré map, as seen in Fig. 3. This fact is explicitly shown for the fixed points of rotation number $2m/1$, at which the Jacobian matrix B of S is given by

$$B=\begin{bmatrix}1 & a\\ b & 1+ab\end{bmatrix}\begin{bmatrix}1 & -a\\ b & 1-ab\end{bmatrix}\begin{bmatrix}1 & -a\\ b & 1-ab\end{bmatrix}\begin{bmatrix}1 & a\\ b & 1+ab\end{bmatrix}$$
$$=\begin{bmatrix}1-3a^{2}b^{2}-a^{3}b^{3} & 2a^{2}b-2a^{3}b^{2}-a^{4}b^{3}\\ -4b-4ab^{2}+2a^{2}b^{3}+a^{3}b^{4} & 1-5a^{2}b^{2}+a^{3}b^{3}+a^{4}b^{4}\end{bmatrix} , \tag{27}$$

where

$$a=\pm\frac{\varepsilon\pi}{T}\mathrm{csch}\left[\frac{\pi}{2T}\right] \text{ and } b=\pm\frac{1}{4\pi}e^{m\pi T} . \tag{28}$$

Therefore, the residue can be calculated exactly as follows:

$$R_{2m/1}=\tfrac{1}{4}(8a^{2}b^{2}-a^{4}b^{4}) . \tag{29}$$

From the condition $R_{2m/1}>1$, the elliptic islands or the resonance bands of rotation number $2m/1$ should be found in the region of

$$|H|>\frac{\varepsilon\,\mathrm{csch}\left[\frac{\pi}{2T}\right]}{2(\sqrt{3}-1)T^{2}} . \tag{30}$$

C. The estimate of the width of the stochastic layer

It is necessary to calculate the width of the stochastic layer to compute the diffusion constant of the global transport along the stochastic layer. A rigorous estimate for the width can be obtained by applying Mather's method to the separatrix map. If an invariant circle is a closed loop that encircles the cylinder we call this the *rotational invariant circle* (RIC). The boundaries of the stochastic layer are the outermost RIC of S, which determines the width of the stochastic layer. Birkhoff showed that the RIC of the twist map is a Lipschitz graph $\{Y(t),t\}$ of some continuous function Y [31]. Using the fact that the RIC is a Lipschitz graph, Mather obtained the criterion for the nonexistence of the RIC for the standard map [32]. An application of his method to our problem gives the following rigorous lower bound for the half width W_h (see Appendix A):

$$W_h\geq\frac{3}{8}\frac{\varepsilon}{T^{2}}\mathrm{csch}\left[\frac{\pi}{2T}\right] . \tag{31}$$

But in order to calculate the diffusion constant accurately the above lower bound is not sufficient. Therefore, in order to estimate the width more accurately we use the

Greene's residue criterion [11] for the existence and nonexistence of the RIC:

Criterion. Given two neighboring rationals p/q, p'/q', i.e., $pq'-qp'=\pm 1$, there exists no rotational invariant circles of rotation number between p/q and p'/q' if the residue $R_{p/q}$ and $R_{p'/q'}$ are significantly greater than 0.25. If the residues are significantly smaller then such circles do exist.

From the residue criterion we know that the boundary circle is located between two elliptic periodic orbits corresponding to neighboring rationals with non-negative residue near 0.25. Since in our case the boundary circle determining the stochastic layer is located between two elliptic islands of rotation numbers $2m/1$ and $(2m+2)/1$, which are very close, we can get an estimate of W_h by applying the residue criterion on $R_{2m/1}$ and $R_{2m+2/1}$ though $2m/1$ and $(2m+2)/1$ are not neighboring rationals. The condition $R_{2m/1} \geq \frac{1}{4}$ gives the halfwidth of the stochastic layer W_h

$$|H| \geq \frac{\varepsilon}{\sqrt{10}-\sqrt{6}} \frac{1}{T^2} \operatorname{csch}\left[\frac{\pi}{2T}\right] = W_h \ , \tag{32}$$

which is a much better estimate of the halfwidth than one in Eq. (31). We note that the ratio between W_h and $\varepsilon M_0(T)$ in Eq. (11) is given by

$$\frac{W_h}{\varepsilon M_0(T)} = \frac{2}{(\sqrt{10}-\sqrt{6})T} \ , \tag{33}$$

which indicates that W_h is significantly larger than $\varepsilon M_0(T)$ when T is small. Figure 4 shows the comparison between the analytical estimate in Eq. (32) and the results of numerical simulations by direct integrations of Eq. (3) and iterations of the separatrix map in Eq. (19), which shows excellent agreements between various estimates over a range of T.

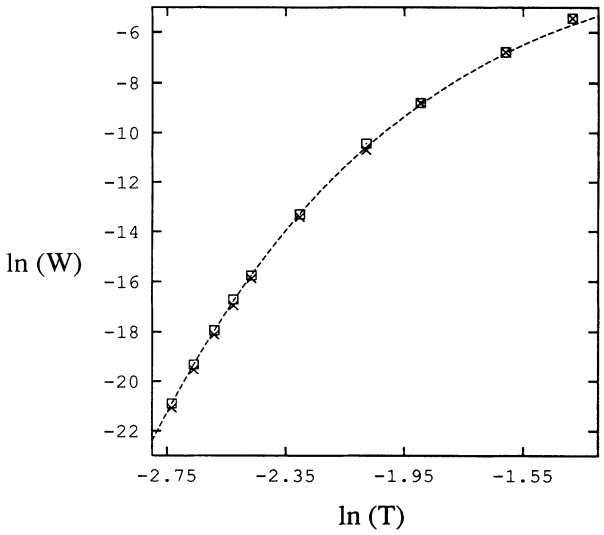

FIG. 4. The width of the stochastic layer with $\varepsilon=0.02$. The analytical results from Eq. (32) are shown in a dotted line and the numerical results from the direct integration and the iterations of the separatrix map in squares and crosses, respectively.

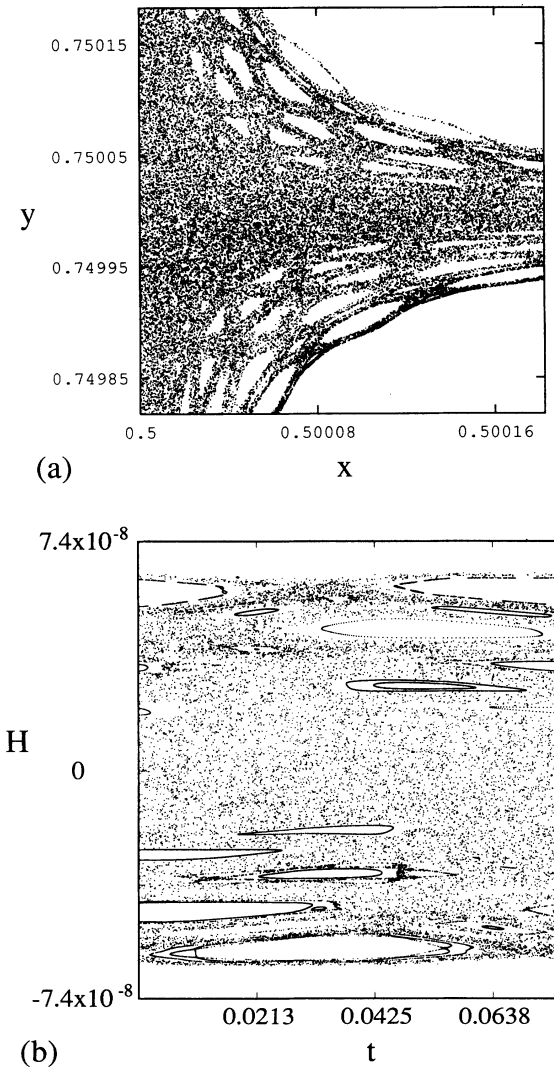

FIG. 3. The phase portrait of the time-T Poincaré map near a saddle point is shown in (a) and the phase portrait of the composite separatrix map S in (b) with $\varepsilon=0.02$, and $T=0.085$. These phase portraits, though in different coordinate systems, show clearly the correspondence between island structures.

IV. THE RANDOM PHASE MODEL AND THE GLOBAL DIFFUSION CONSTANT

A. The random phase assumption

We now consider the problem of the calculation of the global diffusion constant in the stochastic layer. Typically, a fluid particle in the stochastic layer displays chaotic oscillations in one cell for some periods before crossing the separatrix and displaying chaotic oscillations in a neighboring cell. Therefore it is natural to consider the global motion in the stochastic layer as the random walks over the cells. Lichtenberg and Wood [9] used this idea to calculate the diffusion constant for charged particles in a periodic magnetic field along the stochastic web with the assumption that dynamics in the stochastic layer is completely random, that is, the phase space within the

stochastic layer is equally populated on each step of the separatrix map. But this assumption is not adequate for the case of small T because the changes in H per one mapping step is limited by $\varepsilon M_0(T)$ which is significantly smaller than the width of the stochastic layer. As an alternative we consider only t as a random variable, which is called the *random phase assumption.* From Eq. (19) we see that if $|H'|\to 0$, then $t'-t\to\infty$, so that this assumption is reasonable near the separatrix.

With the random phase assumption we have a random model describing the dynamics of H as follows:

$$H'=H+\varepsilon M_0(T)\cos\xi, \quad |H|<W_h \tag{34}$$

where ξ is a random variable in $[0,2\pi]$.

B. The diffusion and correlated random walks

When the sign of H changes the fluid particle crosses the separatrix. Since the crossing is regarded as one random walk step, it is important to know that statistics of the separatrix crossing. The random model gives a set of probabilities P_i that a next crossing occurs at the ith iteration of the map after a separatrix crossing. We note that P_i does not depend on $\varepsilon M_0(T)$ and W_h for small i because W_h is significantly larger than $\varepsilon M_0(T)$ in our consideration. Due to the square lattice geometry of the separatrices dynamics of H leads to dynamics of fluid particles from one cell to another. Since each cell has four separatrices, the probabilities for separatrix crossings P_i, give a set of new probabilities $\tilde{P}_1$, $\tilde{P}_2$, $\tilde{P}_3$, and $\tilde{P}_4$ for a particle moving from one cell to the neighbor through one of four separatrices enclosing a cell (see Fig. 5).

The random phase assumption is not correct in the region with elliptic islands. Therefore, it follows that the tails of the distribution of P_i's for the random model and the separatrix map can be different since there exist orbits confined in one cell for a very long time due to the stickiness of elliptic islands and the effect of cantori as partial barriers for transport. But the $\tilde{P}_i$'s are almost independent of the structure of the layer since the tails of the distribution of P_i contributes almost uniformly to $\tilde{P}_i$, so that $\tilde{P}_i$ is mostly determined by the distribution of P_i for small

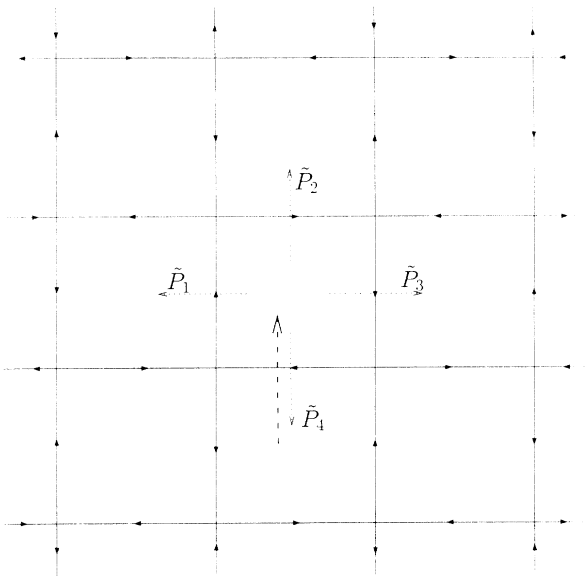

FIG. 5. The correlated random walk model for the global transport describing the cell to cell dynamics. The dashed arrow represents the entering direction of a fluid particle into a cell and $\tilde{P}_i$ are the transition probabilities to the neighboring cells.

i which are related only to the dynamics near the separatrix. Table I provides a comparison between values of P_i and $\tilde{P}_i$ computed numerically by the separatrix map, the direct integration and from the random model in Eq. (34) for various values of T with $\varepsilon=0.02$. Note that the dependence of P_i and $\tilde{P}_i$ on T is small and two sets of values from the separatrix map and from the numerical integrations show excellent agreements.

The differing values of $\tilde{P}_i$'s in Table I imply that the random process over the cell is not a random walk but a *correlated random walk* in which the transition probabilities depend on the entering direction and the rotating direction of the cell. The fluid particle is more likely to exit through the separatrix which it followed closely earlier. This correlation over two successive steps causes fluid particles to persist in the similar direction along the

TABLE I. The probabilities of the separatrix crossing at the ith iteration P_i and the probabilities of the fluid particle jumping from one cell to another, $\tilde{P}_i$, $i=1,2,3,4$ are computed by numerical simulations with the separatrix map and direct integrations of Hamilton's equation of motion for a set of periods, T. They are compared with values given by the random model in Eq. (34), which shows good agreement.

$\varepsilon=0.02$	T	P_1	P_2	P_3	P_4	$\tilde{P}_1$	$\tilde{P}_2$	$\tilde{P}_3$	$\tilde{P}_4$
The	0.085	0.362	0.113	0.073	0.048	0.482	0.218	0.168	0.132
separatrix	0.1	0.336	0.112	0.073	0.050	0.489	0.214	0.165	0.132
map	0.16	0.368	0.109	0.090	0.043	0.479	0.209	0.183	0.129
The	0.085	0.362	0.113	0.073	0.048	0.481	0.215	0.165	0.130
numerical	0.1	0.364	0.111	0.073	0.050	0.487	0.211	0.162	0.131
integration	0.16	0.366	0.109	0.088	0.043	0.478	0.209	0.181	0.130
Random model		0.363	0.112	0.075	0.048	0.480	0.215	0.170	0.135

zig-zag path for a few steps. The correlated random walks still lead to the normal Einstein diffusion where the mean square distance is linearly proportional to the number of steps. The effect of correlation conspicuously appears in the speed of the diffusion, so that the correlated random walk leads only to modification of the diffusion constant. The ratio of diffusion constants between the correlated and uncorrelated random walks is called the *correlation factor* denoted by f_c [13]. If the (u,v) are the coordinates of a particle after N random walk steps, the mean square distance of the two-dimensional correlated random walk is given by

$$L_{\rm MS}=\langle u^2+v^2\rangle=f_c L_s^2 N \ , \tag{35}$$

where L_s is a length of one random walk step and the angular bracket represents the ensemble average. The random model probabilities $\tilde{P}_1$, $\tilde{P}_2$, $\tilde{P}_3$, $\tilde{P}_4$ in Table I yield $f_c \simeq 1.4$ with $L_s=\frac{1}{2}$.

C. The calculation of the diffusion constant

In order to know the time dependence of $L_{\rm MS}$ we need to know the average period of chaotic oscillations within the stochastic layer, $\tau_{\rm av}$, and the average number of random walk steps of particles after J iterations of the separatrix map, $n_{\rm rw}(J)$. If we know these quantities, a straightforward argument gives

$$L_{\rm MS}=f_c L_s^2 \frac{n_{\rm rw}(J)}{J}\frac{4}{\tau_{\rm av}}t \tag{36}$$

and the diffusion constant D

$$D=\frac{L_{\rm MS}}{t}=f_c L_s^2 \frac{n_{\rm rw}(J)}{J}\frac{4}{\tau_{\rm av}} \ , \tag{37}$$

where $\tau_{\rm av}$ is obtained by averaging $T(H)$ over the separatrix layer

$$\tau_{\rm av}=\frac{1}{W_h}\int_0^{W_h}\frac{2}{\pi}\ln\frac{2}{\pi H}dH$$
$$=\frac{2}{\pi}\left[1-\ln\frac{\varepsilon\pi}{2(\sqrt{10}-\sqrt{6})T^2}+\ln\sinh\frac{\pi}{2T}\right] . \tag{38}$$

In order to perform an accurate calculation we need to exclude the elliptic islands within the layer, so that Eq. (38) yields values slightly smaller than accurate ones, but this difference is negligible in calculating the diffusion constant. Remarkably, $n_{\rm rw}(J)/J$ is determined only by the ratio between the area of the stochastic layer and the area crossing the separatrix under one iteration of the separatrix map, so that we get

$$\frac{n_{\rm rw}(J)}{J}=\frac{2\varepsilon M_0(T)T}{\pi S(\varepsilon,T)} \ , \tag{39}$$

where $S(\varepsilon,T)$ is the area of the stochastic layer in the phase space of the separatrix map. This is proved in Appendix B. This property implies that the global diffusion constant is not affected by the stickiness of elliptic islands and the cantori in the stochastic layer except the area considerations of the elliptic islands in the phase space of the separatrix map.

We compute $S(\varepsilon,T)$ by subtracting the area of the elliptic islands within the stochastic layer from the area of the region between two boundary circles determining the stochastic layer, $2W_hT$. Therefore, we define a quantity by

$$\sigma(\varepsilon,T)=\frac{1}{\sqrt{10}-\sqrt{6}}\frac{S(\varepsilon T)}{W_hT}=\frac{S(\varepsilon,T)T}{\varepsilon}\sinh\left[\frac{\pi}{2T}\right] , \tag{40}$$

which is proportional to the ratio between the total area of the stochastic layer without elliptic islands and $2W_hT$. When T is small $\sigma(\varepsilon,T)$ does not depend much on the parameters. If T is not sufficiently small, then $\sigma(\varepsilon,T)$ depends on T in a complicated manner. Table II shows numerically computed values of $\sigma(\varepsilon,T)$ for various values of T, which indicates that $\sigma(\varepsilon,T)$ is roughly constant. This table also provides a comparison between the values of $n_{\rm rw}(J)/J$ obtained by the relation

$$\frac{n_{\rm rw}(J)}{J}=\frac{T}{\sigma(\varepsilon,T)\pi} \tag{41}$$

and the numerical evaluations by the direct integration, which confirms the validity of Eq. (39).

The numerical observations in Table II suggests that $\sigma(\varepsilon,T)\simeq 2.3$, so that we get

$$S(\varepsilon,T)\simeq 2.3\frac{\varepsilon}{T}\,\mathrm{csch}\left[\frac{\pi}{2T}\right] . \tag{42}$$

Therefore, the analytic estimates of $L_{\rm MS}$ and D are given by

TABLE II. The area $S(\varepsilon,T)$ is computed numerically with $\varepsilon=0.02$, from which $n_{\rm rw}(J)/J$ is computed by using Eq. (39) and compared with the results of numerical simulations.

T	$\sigma(\varepsilon,T)$	$\frac{1}{J}n_{\rm rw}(J)$ from Eq. (39)	Numerical values of $\frac{1}{J}n_{\rm rw}(J)$
0.075	2.270	0.01052	0.01075
0.1	2.238	0.01422	0.01475
0.13	2.433	0.01701	0.01778
0.16	2.265	0.02249	0.02299
0.2	2.363	0.02694	0.02786

$$L_{\mathrm{MS}}=f_c L_s^2 \frac{T}{\sigma(\varepsilon,T)\pi}\frac{4}{\tau_{\mathrm{av}}}t$$

$$\simeq \frac{f_c}{2.3}\frac{Tt}{2\left[1-\ln\frac{e\pi}{2(\sqrt{10}-\sqrt{6})T^2}+\ln\sinh\frac{\pi}{2T}\right]} \quad (43)$$

and

$$D=\frac{L_{\mathrm{MS}}}{t}=\frac{f_c}{2.3}\frac{T}{2\left[1-\ln\frac{e\pi}{2(\sqrt{10}-\sqrt{6})T^2}+\ln\sinh\frac{\pi}{2T}\right]}, \quad (44)$$

with the correlation factor $f_c \sim 1.4$ from Table I.

Figure 6 provides a comparison of L_{MS} obtained by numerical simulations with the separatrix map and the direct integration using the fourth order Runge-Kutta method with the time step of 0.005. The ensemble average is done over 1900 fluid particles initially distributed uniformly in the stochastic layer for the direct integration and over 10 000 fluid particles for the separatrix map with 10 000 iterations of the separatrix map. The L_{MS} from direct integration shows larger fluctuations due to the smaller number of ensembles taken for the average. After same transient behavior, the slope of two curves converge, which demonstrates good agreements between results of the separatrix map and the direct numerical integrations.

In order to get an accurate value of the diffusion constant, fluid particles must be distributed uniformly in the stochastic layer. But due to the effect of the islands and the cantori it may take a very long time for fluid particles starting near the separatrix to fill the whole stochastic layer uniformly. Numerical results indicate that it needs at least 10^6 iterations for our parameter values to achieve this uniformity, which results in the extremely slow convergence of the diffusion constant, as seen in Fig. 7. Consequently, it is difficult to get the accurate diffusion constant by the direct integration with our computational

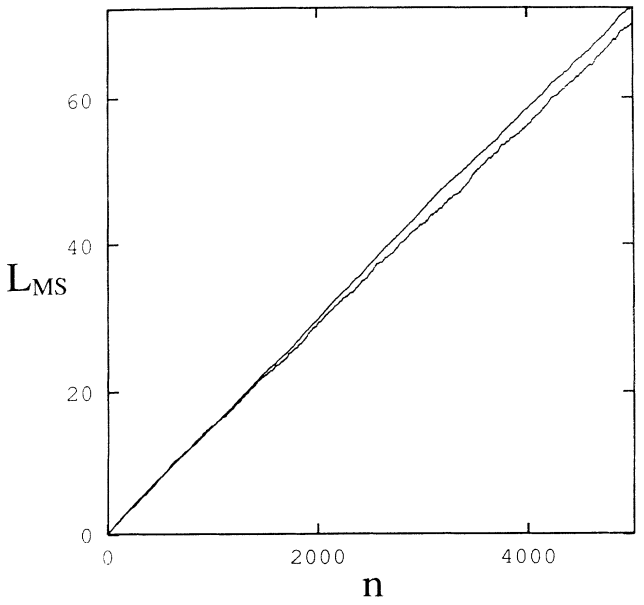

FIG. 6. The plot of the number of iterations, n, versus L_{MS} from direct integrations of Hamilton's equation of motion and iterations of the separatrix map with $\varepsilon=0.02$ and $T=0.125$. The curve from direct integrations (below) shows more fluctuations since the size of the ensemble is about five times smaller than one from the separatrix map.

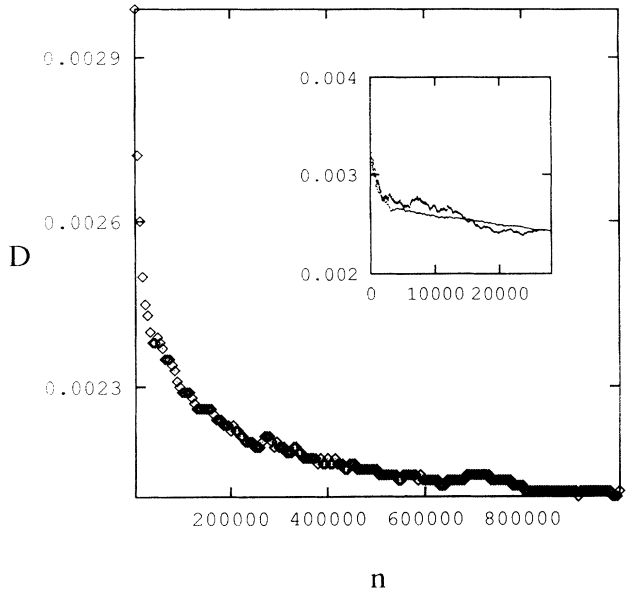

FIG. 7. The plot of the number of iterations n versus the diffusion constant D computed from the separatrix map when $\varepsilon=0.02$ and $T=0.1$, which shows the extremely slow convergence. The inset shows the initial comparison between the diffusion constants from numerical integration and the separatrix map.

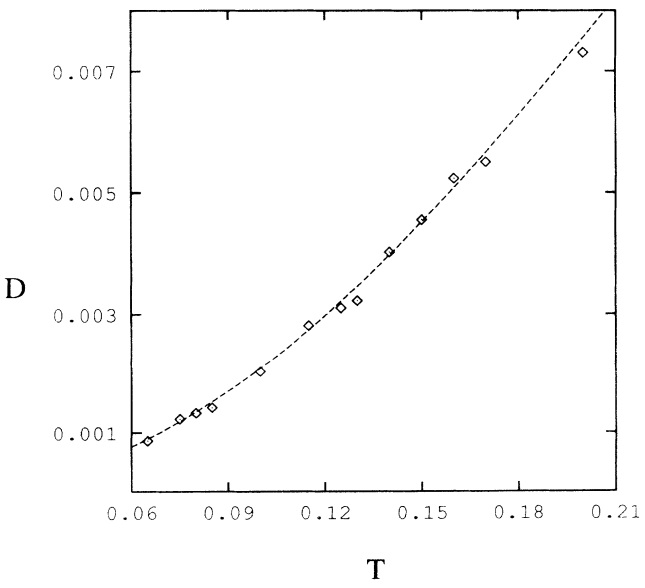

FIG. 8. The diffusion constant computed from Eq. (44) is shown in a solid line and one from iterations of the separatrix map in diamonds, which are in excellent agreement.

power since computational efforts increase as T decreases. Therefore the separatrix map is used heavily in studying the diffusion numerically. The initial values of diffusion constants from direct integrations and iterations of the separatrix map are shown in the inset of Fig. 7, which are in good agreement and exhibit similar convergence behaviors. Figure 8 shows the comparison between the analytical results from Eq. (44) and the numerical ones from iterations of the separatrix map. The numerical results are obtained from the ensemble average over 10 000 fluid particles distributed in the stochastic layer iterated 10^6 times by the separatrix map. The analytically and numerically computed diffusion constants show excellent agreements, confirming the validity of the use of the separatrix map and the random phase assumption.

V. CONCLUSION AND DISCUSSIONS

In the planar periodic vortical flow described by the time-dependent stream function, fluid particles can be transported along the globally connected stochastic web. By considering the separatrix map and applying the theory of twist maps to the separatrix map we get analytic expressions for the width of the stochastic layer and the global diffusion constant, which are in good agreements with numerical simulations.

Since the separatrix map yields a large error in the phase t near the separatrix, it may appear that it cannot describe the long-time dynamics of one fluid particle. But, since the phase t can be regarded as a random variable, the separatrix map gives the accurate probabilities for separatrix crossings, so that the use of the separatrix map for studying the transport problem is valid. In particular, when T is small, there are several advantages of using the separatrix map. It gives a quite accurate estimate for the diffusion constant because the dynamics is described by the model with random phase. Remarkably, the long-time correlations near the invariant circles or the cantori do not have a direct influence on the diffusion constant except that their areas have to be counted out. This fact was also mentioned by Lichtenberg and Wood [9] in the context of the random model. The random phase assumption leads to the global transport modeled by correlated random walks from one cell to another. In fact, the difference of the diffusion constant between the original Hamiltonian system and the separatrix map is mainly due to the errors in the transition probabilities of the correlated random walks, the average period of chaotic oscillations $\tau_{\rm av}$, and the areas of the phase space available for global transport and the regions that cross the separatrix by one iteration of the map, which can be obtained accurately with very small errors (from Table II).

For the case of small ε and T, the diffusion is a normal Einstein diffusion and no accelerator mode has been found, the existence of which changes the nature of the diffusion to anomalous. It should be interesting to study the limit of large ε to pursue the possibility of finding these modes by looking at the phase portraits and numerically computing the diffusion constants as a function of ε [2].

ACKNOWLEDGMENTS

We would like to thank Professor Yup Kim for helpful remarks and Professor H. Mori for valuable comments on the paper. This work was supported in part by the Basic Science Research Institute at POSTECH under Contract No. N91126 and in part by KOSEF through the Global Analysis Research Center.

APPENDIX A

Applying Birkhoff's theorem to each $S^{\pm}$ in Eq. (19) it is easily seen that the rotating invariant circle (RIC) of S is a Lipschitz graph and there exist four different Lipschitz functions $Y_i(t)$, $(i=1,\ldots,4)$ representing the images of the RIC of S under successive iterations of $S^{\pm}$. Following Mather [32], there exist almost everywhere differentiable Lipschitz homeomorphisms $g_i: T^1 \to \mathbb{R}$, $i \in \mathbb{Z}_4 = \{0,\ldots,3\}$ such that

$$S^{\pm}(t, Y_i(t)) = [g_i(t), Y_{i+1}(g_i(t))] \ . \tag{A1}$$

For a notational convenience, we omit the subscript i of g and assume that the RIC is located in the region with $H' > 0$. With the generating function $G(t,t')$ for the periodic vortical flow in Eq. (20) we have

$$\frac{\partial}{\partial t}[G(\bar{t},t)+G(t,t')]=0 \ , \tag{A2}$$

where $\bar{t}=g^{-1}(t)$, $t'=g(t)$, or,

$$-\frac{2}{\pi}e^{2\pi[g^{-1}(t)-t]}+\frac{2}{\pi}e^{2\pi[t-g(t)]} \mp \varepsilon M_0(T)\cos\left[\frac{2\pi}{T}t\right]=0 \ . \tag{A3}$$

By differentiating (A3), we obtain

$$-2\pi H\left[\frac{dg^{-1}}{dt}-1\right]+2\pi H'\left[1-\frac{dg}{dt}\right]\pm B\sin\frac{2\pi}{T}t=0 \ , \tag{A4}$$

or

$$2\pi H\frac{dg^{-1}}{dt}+2\pi H'\frac{dg}{dt}=2\pi(H+H')\pm B\sin\frac{2\pi}{T}t \ , \tag{A5}$$

where

$$B=\frac{2\pi}{T}\varepsilon M_0(T), \quad H=\frac{\partial G}{\partial t}(t,t') \ , \quad \text{and } H'=-\frac{\partial G}{\partial t'}(t,t') \ . \tag{A6}$$

We note that $H'=H\pm\varepsilon M_0(T)\cos[(2\pi/T)t]$ and hence $H=H'$ when $t=\frac{3}{4}T$.

Let L be the larger of the Lipschitz constants of g and g^{-1}, i.e.,

$$L=\max\left\{\sup\frac{|g(t)-g(t')|}{|t-t'|},\sup\frac{|g^{-1}(t)-g^{-1}(t')|}{|t-t'|}\right\} . \tag{A7}$$

In view of the definition of L, it follows that

$$L^{-1} \le \frac{dg}{dt} \le L, \quad L^{-1} \le \frac{dg^{-1}}{dt} \le L \ . \tag{A8}$$

From (A5) and (A7) we get

$$2\pi H L^{-1} + 2\pi H' L^{-1} \le 2\pi(H+H') - B \ , \tag{A9}$$

and when $t = 3T/4$,

$$L^{-1} \le 1 - \frac{B}{4\pi H} \ . \tag{A10}$$

From the definition of L and the theory of functions [33], we also get

$$L = \max\left\{ \text{ess.sup}\frac{dg(t)}{dt}, \text{ess.sup}\frac{dg^{-1}(t)}{dt} \right\} . \tag{A11}$$

Here ess.sup means "essential supremum" in the sense of measure theory. From (A5), (A8), and (A11) we get

$$2\pi H L^{-1} + 2\pi H' L \le 2\pi(H+H') + B \ . \tag{A12}$$

In particular, when $t = 3T/4$, we get

$$L^{-1} + L \le 2 + \frac{B}{2\pi H} \ . \tag{A13}$$

Since the function $L^{-1}+L$ is a monotone increasing function for $L \ge 1$,

$$\frac{4\pi H - B}{4\pi H} + \frac{4\pi H}{4\pi H - B} \le 2 + \frac{B}{2\pi H} \tag{A14}$$

or

$$H \ge \frac{3}{8\pi} B = \varepsilon \frac{3\pi}{8T^2} \text{csch}\left[\frac{\pi}{2T} \right] . \tag{A15}$$

APPENDIX B

Let S be an area-preserving map on the cylinder $T^1 \times \mathbb{R} = (\mathbb{R}/\mathbb{Z}) \times \mathbb{R}$ and U be an open invariant set with finite area. For a rotational circle C contained in U we define the subset A of U by the set of points which cross C by one iteration of S, that is, x and Sx are located on different sides of C. The average number of crossing C after J iterations of S, denoted by $n_{\text{au}}(J)$, is given by

$$n_{\text{av}}(J) = \frac{1}{|U|} \int_U n(x;J) dx \ , \tag{B1}$$

where $n(x;J)$ is the frequency that a point x crosses C while S is iterated J times and $|U|$ is the area of U.

From the definition of A we have a recurrent relation on $n(x;J)$

$$n(x;J) = \begin{cases} n(x;J-1)+1 & \text{if } x \in A \\ n(x;J-1) & \text{if } x \notin A \end{cases} \tag{B2}$$

and, in particular, when $J = 1$

$$n(x;1) = \begin{cases} 1 & \text{if } x \in A \\ 0 & \text{if } x \notin A \ . \end{cases} \tag{B3}$$

Thus $n_{\text{av}}(J)$ has a following recurrent relation

$$\begin{aligned} n_{\text{av}}(J) &= \frac{1}{|U|} \int_{U \setminus A} n(x;J-1) dx \\ &\quad + \frac{1}{|U|} \int_A [n(x;J-1)+1] dx \\ &= n_{\text{av}}(J-1) + \frac{|A|}{|U|} \end{aligned} \tag{B4}$$

with the initial condition

$$n_{\text{av}}(1) = \frac{|A|}{|U|} \ . \tag{B5}$$

Consequently, we have

$$n_{\text{av}}(J) = J \frac{|A|}{|U|} \ . \tag{B6}$$

For our system, we have

$$|U| = S(\varepsilon, T) \text{ and } |A| = \frac{2T}{\pi} \varepsilon M_0(T) \ , \tag{B7}$$

which yields

$$\frac{n_{\text{rw}}(J)}{J} = \frac{2\varepsilon M_0(T) T}{\pi S(\varepsilon, T)} \ . \tag{B8}$$

[1] J. B. Weiss and E. Knobloch, Phys. Rev. A **40**, 2579 (1989).
[2] K. Ouchi and H. Mori, Prog. Theor. Phys. **88**, 467 (1991).
[3] R. Camassa and S. Wiggins, Phys. Rev. A **43**, 774 (1991).
[4] J. M. Ottino, *The Kinematics of Mixing: Stretching, Chaos and Transport* (Cambridge University Press, Cambridge, 1989).
[5] A. L. Bertozzi, SIAM J. Math. Anal. **19**, 1271 (1988).
[6] J. Pedlosky, *Geophysical Fluid Dynamics* (Springer-Verlag, New York, 1982).
[7] B. V. Chirikov, Phys. Rep. **52**, 263 (1979).
[8] D. F. Escande, in *Plasma Theory and Nonlinear and Turbulent Process in Physics,* edited by N. S. Erkohin, A. G. Sitenko, and V. E. Zakharov (World Scientific, Singapore, 1988), p. 398.
[9] A. J. Lichtenberg and B. P. Wood, Phys. Rev. A **39**, 2153 (1989).
[10] V. V. Afanasiev, A. A. Chernikov, R. Z. Sagdeev, and G. M. Zaslavsky, Phys. Lett. A **144**, 229 (1990).
[11] J. M. Greene, J. Math. Phys. **20**, 1183 (1979).
[12] V. Rom-Kedar, Physica D **43**, 229 (1990).
[13] J. W. Haus and K. W. Kehr, Phys. Rep. **150**, 264 (1987).
[14] R. S. Mackay, J. D. Meiss, and I. C. Percival, Physica D **13**, 55 (1984).
[15] J. D. Meiss and E. Ott, Physica D **20**, 387 (1986).
[16] V. Rom-Kedar, A. Leonard, and S. Wiggins, J. Fluid Mech. **214**, 347 (1990).
[17] V. Rom-Kedar and S. Wiggins, Arch. Rational Mech. Anal. **109**, 239 (1990).
[18] V. Rom-Kedar and S. Wiggins, Physica D **51**, 248 (1991).
[19] V. K. Melnikov, Trans. Moscow Math. Soc. **12**, 1 (1963).
[20] J. Guckenheimer and P. J. Holmes, *Nonlinear Oscillations,*

Dynamical Systems, and Bifurcations of Vector Fields (Springer-Verlag, New York, 1983).
[21] S. Smale, in *Differential and Combinatorial Topology,* edited by S. S. Carins (Princeton University Press, Princeton, 1963).
[22] G. D. Birkhoff, Mem. Pont. Acad. Sci. Novi Lyncaei **1**, 85 (1935).
[23] P. J. Holmes, J. E. Marsden, and J. Scheurle, Contemp. Math. **81**, 213 (1988).
[24] E. Fontich and C. Simo, Ergod. Theory Dyn. Syst. **10**, 295 (1990).
[25] J. Marsden, R. Montgomery, and T. Ratiu, Contemp. Math. **97**, 299 (1990).
[26] J. D. Meiss, Rev. Mod. Phys. **64**, 795 (1992).
[27] S. Aubry, Physica D **7**, 240 (1983).
[28] J. N. Mather, Topology **21**, 457 (1982).
[29] A. Katok, Ergod. Theory Dyn. Syst. **2**, 185 (1982).
[30] S. Wiggins, *Introduction to Applied Nonlinear Dynamical Systems and Chaos* (Springer-Verlag, New York, 1990).
[31] G. R. Birkhoff, Acta Math. **43**, 1 (1920).
[32] J. N. Mather, Ergod. Theory Dyn. Syst. **4**, 301 (1984).
[33] E. C. Titchmarsh, *The Theory of Functions* (Oxford University Press, Oxford, 1939), Chap. 11.7.

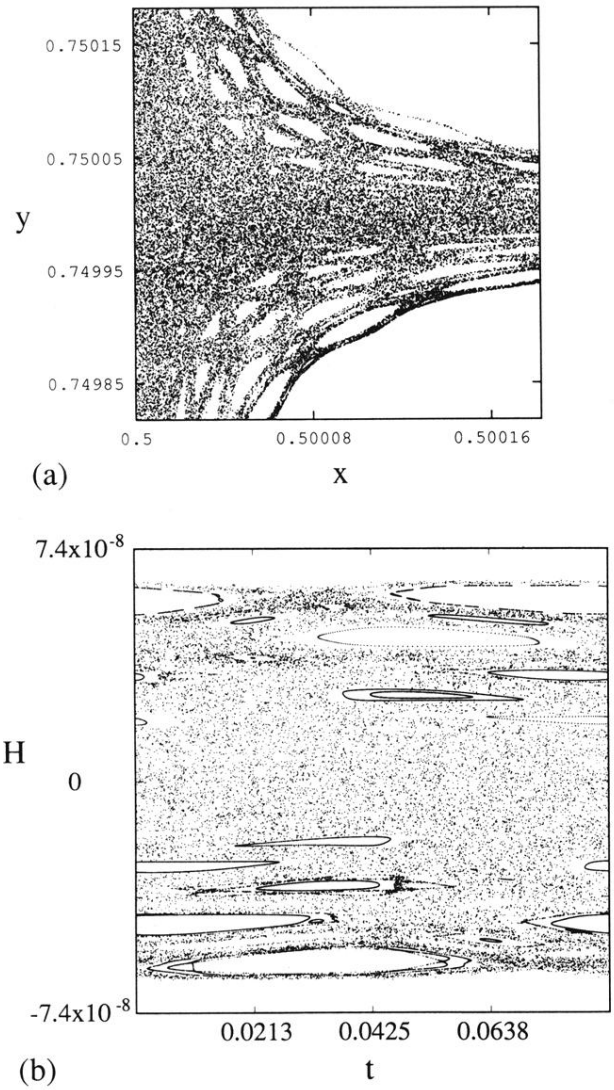

FIG. 3. The phase portrait of the time-T Poincaré map near a saddle point is shown in (a) and the phase portrait of the composite separatrix map S in (b) with $\varepsilon=0.02$, and $T=0.085$. These phase portraits, though in different coordinate systems, show clearly the correspondence between island structures.